

Cyclin A regulates kinetochore microtubules to promote faithful chromosome segregation

Lilian Kabeche^{1,2} & Duane A. Compton^{1,2}

The most conspicuous event in the cell cycle is the alignment of chromosomes in metaphase. Chromosome alignment fosters faithful segregation through the formation of bi-oriented attachments of kinetochores to spindle microtubules. Notably, numerous kinetochore-microtubule (k-MT) attachment errors are present in early mitosis (prometaphase)¹, and the persistence of those errors is the leading cause of chromosome mis-segregation in aneuploid human tumour cells that continually mis-segregate whole chromosomes and display chromosomal instability²⁻⁷. How robust error correction is achieved in prometaphase to ensure error-free mitosis remains unknown. Here we show that k-MT attachments in prometaphase cells are considerably less stable than in metaphase cells. The switch to more stable k-MT attachments in metaphase requires the proteasome-dependent destruction of cyclin A in prometaphase. Persistent cyclin A expression prevents k-MT stabilization even in cells with aligned chromosomes. By contrast, k-MTs are prematurely stabilized in cyclin-A-deficient cells. Consequently, cells lacking cyclin A display higher rates of chromosome mis-segregation. Thus, the stability of k-MT attachments increases decisively in a coordinated fashion among all chromosomes as cells transit from prometaphase to metaphase. Cyclin A creates a cellular environment that promotes microtubule detachment from kinetochores in prometaphase to ensure efficient error correction and faithful chromosome segregation.

The correction of k-MT attachment errors relies on the detachment of microtubules from kinetochores⁸, and current models for k-MT regulation involve either chromosome-autonomous⁹ or chromosome-coordinated processes (Extended Data Fig. 1). We measured k-MT attachment stability using fluorescence dissipation after photoactivation in three vertebrate cell lines (Fig. 1 and Extended Data Fig. 2). Cells were defined as prometaphase and metaphase on the basis of chromosome alignment using differential interference contrast (DIC) optics. In each cell line the average stability of the stable MT population (for example, k-MTs) in prometaphase was significantly less than in metaphase ($P \leq 0.01$, Student's *t*-test; Fig. 1a-c), and the k-MT half-lives in prometaphase and metaphase cells distributed into non-overlapping populations. The difference cannot be accounted for by differences in the initial intensity of green fluorescent protein (GFP) fluorescence after photoactivation (Extended Data Fig. 3a), the fraction of microtubules in the slowly decaying population (Extended Data Fig. 3b), or poleward microtubule flux (Extended Data Fig. 4). Notably, fluorescence decay of the activated region in both metaphase and prometaphase cells fits to a double exponential curve ($R^2 > 0.99$), indicating that only two populations of microtubules are identified by this method: non-k-MTs and k-MTs¹⁰.

To test whether k-MT attachments become progressively stabilized during prometaphase we measured k-MT stability serially in the same

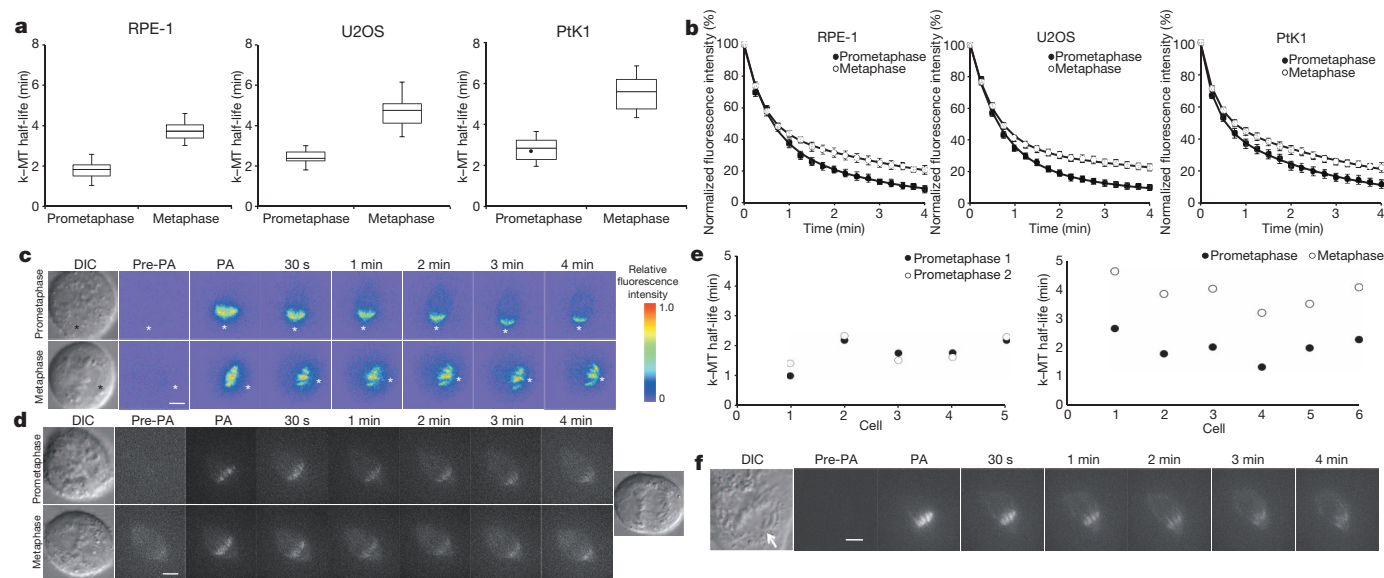


Figure 1 | The stability of k-MT attachments in prometaphase and metaphase. **a**, Box (s.d. of the mean) and whisker (range of data points) plots of k-MT half-lives of RPE-1, U2OS and PtK1 cells expressing photoactivatable GFP-tubulin in prometaphase and metaphase calculated from the fluorescence intensity decay curves ($R^2 > 0.99$); $n = 40$ cells for RPE-1 and U2OS, and 20 cells for PtK1 per condition. Black circle represents the cell in **f**. **b**, Normalized fluorescence intensity of prometaphase (filled circles) and metaphase (white circles) spindles. **c**, DIC and background-subtracted fluorescence images

(pseudo-coloured heat maps) of U2OS cells in prometaphase and metaphase. Asterisks mark spindle poles. Scale bar, 5 μm . PA, photoactivation. **d**, DIC and fluorescence images of an RPE-1 cell in prometaphase and metaphase. Scale bar, 5 μm . **e**, k-MT half-life of individual RPE-1 cells photoactivated serially in prometaphase (left) or in prometaphase and then in metaphase (right). **f**, DIC and fluorescence images of a PtK1 cell in prometaphase. Arrow indicates unaligned chromosome. Scale bar, 5 μm .

¹Department of Biochemistry, Geisel School of Medicine at Dartmouth, Hanover, New Hampshire 03755, USA. ²Norris Cotton Cancer Center, Lebanon, New Hampshire 03756, USA.

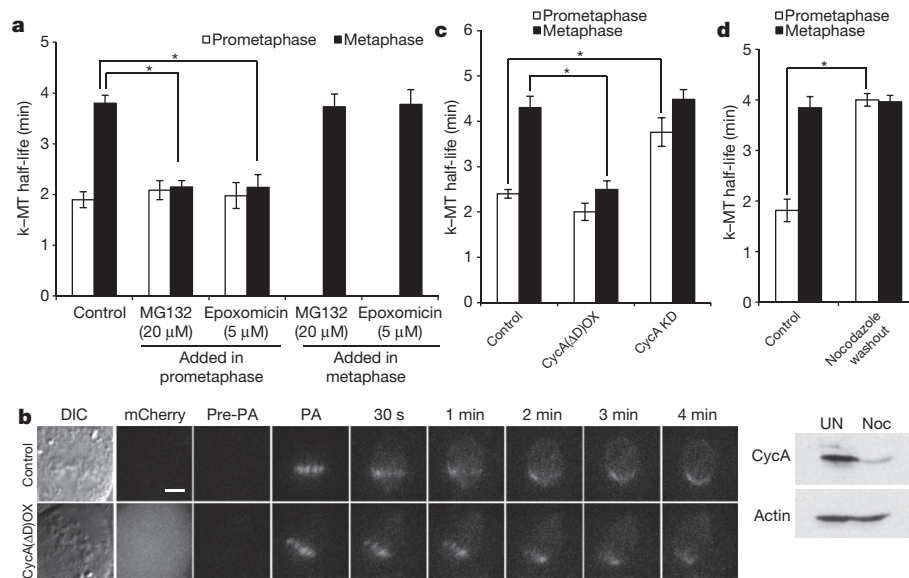


Figure 2 | k-MT stability relies on cyclin A. **a**, k-MT half-life of RPE-1 cells treated with 20 μ M MG132 or 5 μ M epoxomicin in prometaphase and metaphase; $n = 10$ cells per condition. **b**, DIC and fluorescence images of metaphase spindles in untreated (control) and cyclin-A-overexpressing (CycA(Δ D)OX); in which Δ D indicates mutant lacking the destruction box) U2OS cells, with cyclin A(Δ D) visualized by mCherry fluorescence. Scale bar, 5 μ m. **c**, k-MT half-life of untreated (control), cyclin-A-overexpressing and

cyclin-A-depleted (CycA knockdown (KD)) U2OS cells; $n = 13$ cells for control, $n = 10$ cells for CycA(Δ D)OX and CycA KD per condition. **d**, Top, k-MT half-life of RPE-1 cells untreated (control) or released from 12 h nocodazole treatment (nocodazole washout); $n = 10$ cells per condition. Bottom, cyclin A and actin immunoblot of untreated (UN, control) or nocodazole-arrested (Noc) cells. Graphs show mean \pm s.e.m. * $P \leq 0.01$, two-tailed t -test.

cell (Fig. 1d, e). Repeated photoactivation did not compromise cell viability as judged by successful progression to anaphase (Fig. 1d and Extended Data Fig. 5a). Photoactivation of RPE-1 cells twice in prometaphase yielded equivalent k-MT half-lives for each trial in each cell. By contrast, k-MT stability increased sharply between prometaphase and metaphase when measured in the same cell (Fig. 1e). The

switch in k-MT stability was notably consistent at 1.9 ± 0.2 min. Similar results were obtained in U2OS cells (Extended Data Fig. 5b). The percentage of microtubules in the slowly decaying fraction did not change at different times in prometaphase cells (Extended Data Fig. 5c) as would be predicted by the chromosome-autonomous model (Extended Data Fig. 1). We also photoactivated the spindle microtubules of aligned

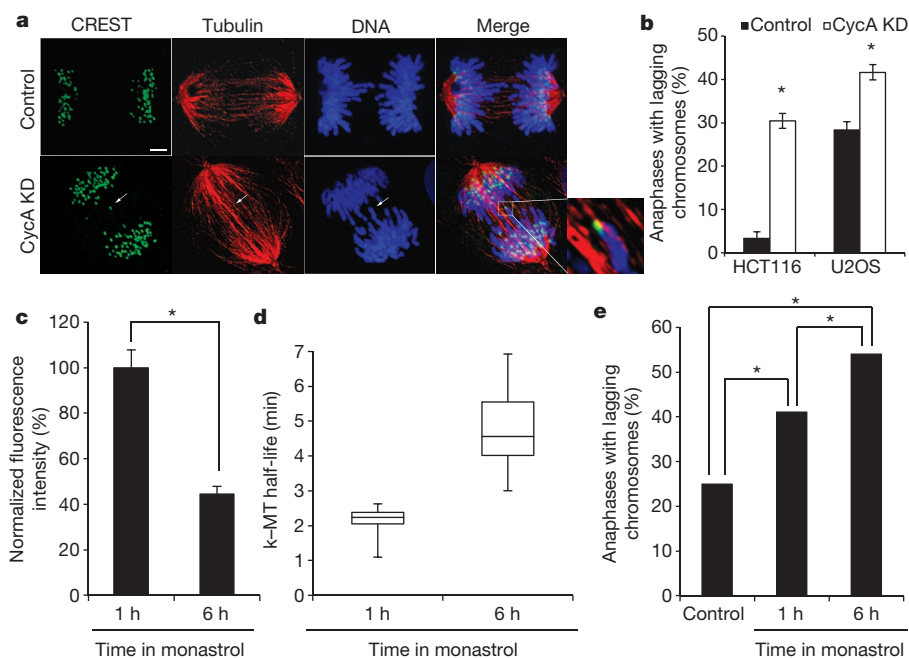


Figure 3 | Cyclin A deficiency increases chromosome mis-segregation. **a**, Anaphase spindles of untreated (control) or cyclin-A-depleted U2OS cells. White arrow highlights merotelic kinetochore. CREST sera is used to mark centromeres. Scale bar, 5 μ m. **b**, Percentage of anaphase cells with lagging chromosomes; $n = 300$ cells per condition from three independent experiments. **c**, Fluorescence intensities of U2OS cells stained for cyclin A;

$n = 100$ cells per condition from three independent experiments. **d**, Box and whisker plot of k-MT half-lives of U2OS cells incubated in monastrol for 1 h and 6 h; $n = 10$ cells per condition. **e**, Percentage of anaphase cells with lagging chromosomes that were untreated (control), or after recovery from monastrol incubation for 1 h or 6 h; $n = 100$ cells for 1 h and 123 cells for 6 h. Graphs show mean \pm s.e.m. * $P \leq 0.01$, two-tailed t -test.

chromosomes in a prometaphase PtK1 cell containing one unaligned chromosome (Fig. 1f). The half-life of k-MTs on these aligned chromosomes in this cell was 2.5 min (single data point identified in Fig. 1a) and within the population of other prometaphase cells. These data demonstrate a coordinated switch in k-MT attachment stability between prometaphase and metaphase cells (Extended Data Fig. 1).

Next, we tested whether the switch in k-MT attachment stability relies on protein turnover (Fig. 2a). Proteasome inhibition did not alter k-MT attachment stability during prometaphase. However, when cells transitioned from prometaphase to metaphase in the presence of the inhibitors the switch to stable k-MT attachments was prevented (Fig. 2a). Proteasome inhibition had no effect if the inhibitors were added after chromosome alignment in metaphase. Cells failed to progress to anaphase in all these conditions, verifying the effective inhibition of the proteasome. Thus, the proteasome-dependent destruction of protein substrates during prometaphase is required for the coordinated switch in k-MT stability in metaphase.

Cyclin A is degraded in prometaphase^{11,12}, and we tested whether cyclin A influenced the switch in k-MT attachment stability (Fig. 2b–d). Expression of an mCherry-tagged mutant version of cyclin A that lacks the degradation box was confirmed by immunoblot (Extended Data Fig. 6a) and shown to persist in mitotic cells by fluorescence microscopy (Fig. 2b). Expression of this mutant cyclin A did not change k-MT attachment stability in prometaphase (Fig. 2c), but prevented the switch to stable attachments in metaphase (Fig. 2b, c and Extended Data Fig. 6c). This mutant version of cyclin A did not impair chromosome bi-orientation as judged by the displacement of the BUB1B (also known as BUBR1) from kinetochores¹³, the recruitment of astrin to kinetochores¹⁴ or the relative inter-kinetochore distance (Extended

Data Fig. 7). The quantity and activity of aurora B kinase^{15,16} was slightly increased in cells overexpressing this mutant of cyclin A during metaphase (Extended Data Fig. 7). There was no apparent linear correlation between k-MT attachment stability and expression level of this protein (Extended Data Fig. 6b), indicating that the persistent expression of cyclin A is sufficient to exceed a threshold that prevents a switch from unstable to stable k-MT attachments.

Vertebrate cells can enter mitosis in the absence of cyclin A^{17,18}, and we depleted cyclin A expression using RNA interference (Extended Data Fig. 6a). Prometaphase cells lacking cyclin A displayed k-MT attachment stability equivalent to untreated metaphase cells (Fig. 2c and Extended Data Fig. 6c). k-MT attachment stability in metaphase cells lacking cyclin A was not different from control cells. There was a slight decrease in the quantity and activity of aurora B kinase during prometaphase (Extended Data Fig. 7). We also prolonged mitosis with nocodazole to allow the destruction of endogenous cyclin A (Fig. 2d), as cyclin A destruction is not prevented by the spindle assembly checkpoint¹⁹. k-MT attachments are significantly more stable in prometaphase cells recovering from nocodazole treatment than untreated control cells (Fig. 2d). Nocodazole recovery did not alter k-MT attachment stability once cells reached metaphase. Manipulation of cyclin A (either depletion or expression of the non-degradable mutant) had no effect on the stability of non-k-MT (Extended Data Fig. 8a) or MT stability in cells lacking the NUF2 protein that lack k-MT (Extended Data Fig. 8b, c) showing that cyclin A specifically influences k-MT. Poleward microtubule flux did not account for the difference in k-MT stability between control cells and cells overexpressing non-degradable cyclin A (Extended Data Fig. 9). Thus, cyclin A destabilizes k-MT attachments to regulate the switch from unstable k-MT in prometaphase to stable k-MT in metaphase.

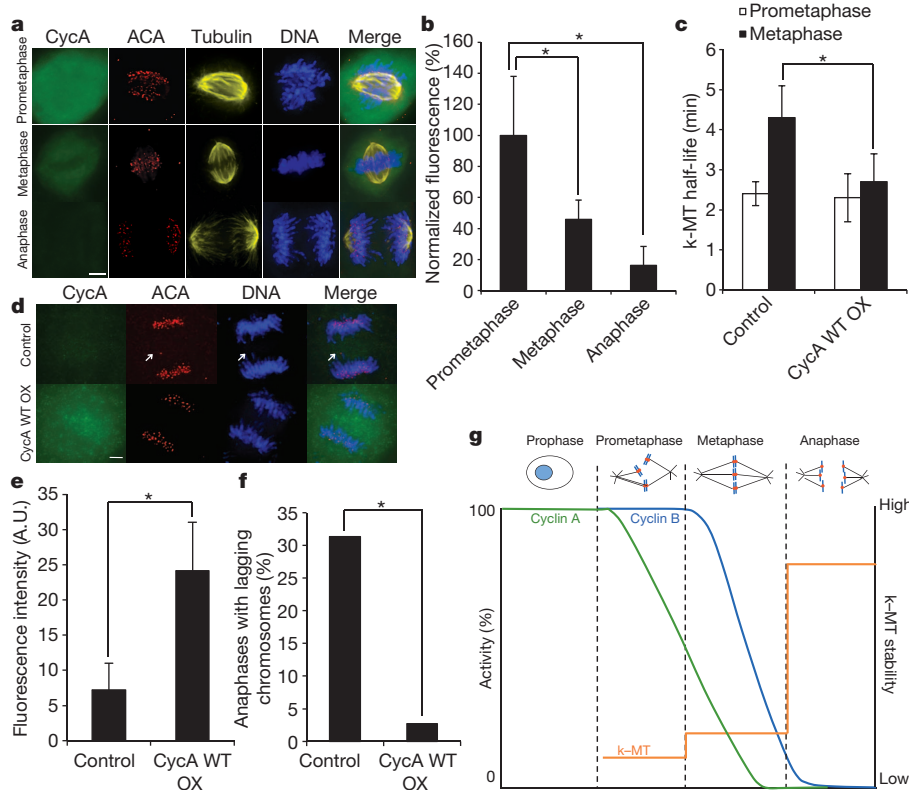


Figure 4 | Cyclin A promotes faithful chromosome segregation.

a, Immunofluorescence of endogenous cyclin A, tubulin, centromeres (ACA) and DNA of U2OS cells in prometaphase, metaphase and anaphase. Scale bar, 5 μ m. **b**, Fluorescence intensities of U2OS cells stained for cyclin A; $n = 150$ cells per condition from three independent experiments. **c**, k-MT half-life of untreated (control) and wild-type cyclin-A-overexpressing (CycA WT OX) U2OS cells; $n = 10$ cells per condition. **d**, Immunofluorescence of endogenous cyclin A, tubulin, centromeres and DNA of control or wild-type-cyclin-A-overexpressing

U2OS cells. Scale bar, 5 μ m. **e**, Fluorescence intensities of cyclin A of control U2OS cells or cells expressing wild-type cyclin A. **f**, Number of anaphases in U2OS cells with lagging chromosomes; $n = 150$ for control cells and 37 for wild-type cyclin A cells. **g**, Cells enter prometaphase with high cyclin A and cyclin B. The proteasome-dependent reduction of cyclin A levels below a critical threshold induces a coordinated increase in k-MT attachment stability at the prometaphase to metaphase transition. Graphs show mean \pm s.e.m. * $P \leq 0.01$, two-tailed *t*-test.

There is a direct relationship between k-MT attachment stability and chromosome segregation fidelity², and cyclin A deficiency led to a significant increase in the fraction of cells displaying lagging chromosomes in anaphase (Fig. 3b). The lagging chromosomes are caused by persistent merotelic kinetochore attachments, as judged by k-MT attachments oriented towards both spindle poles (Fig. 3a). These segregation errors were not caused by alterations in chromosome compaction (Extended Data Fig. 10a, b) or DNA double-strand breaks (Extended Data Fig. 10c). Furthermore, cells arrested in mitosis with monastrol for 6 h display a 60% reduction in cyclin A levels and have significantly more stable k-MT attachments relative to cells arrested for only 1 h (Fig. 3c, d). Accordingly, cells recovering from 6 h of monastrol treatment displayed significantly higher percentages of anaphase cells with lagging chromosomes compared to cells recovering from only 1 h of monastrol treatment (Fig. 3e). Thus, by destabilizing k-MTs cyclin A promotes faithful chromosome segregation, although disruption of the canonical functions of cyclin A during S phase (via short interfering RNA or protein overexpression) could also contribute to the observed chromosome mis-segregation.

Quantitative fluorescence imaging indicates that endogenous cyclin A levels drop to 40% and 20% in metaphase and anaphase, respectively, relative to prometaphase cells (Fig. 4a, b). Thus, the cyclin A level in the prometaphase cell shown in Fig. 1f has yet to dip below that threshold. Expression of wild-type cyclin A tagged with mCherry destabilizes k-MT attachments in metaphase akin to the non-degradable mutant cyclin A (Fig. 4c), but it does not prohibit anaphase entry¹² and we observe anaphase cells with cyclin A levels approximately fourfold higher than untreated cells in anaphase (Fig. 4e). Consequently, chromosome segregation fidelity is increased in cells expressing wild-type cyclin A (Fig. 4f), consistent with previous data showing that the destabilization of k-MT restores faithful chromosome segregation to chromosomally unstable cancer cells².

The stability of k-MT attachments must fall within a narrow permissible range to both satisfy the spindle assembly checkpoint and promote faithful chromosome segregation^{2,20,21}. Our data show that initial k-MT attachments in prometaphase are unstable, yet sufficiently robust to promote chromosome alignment. By maintaining unstable k-MT attachments on bi-oriented chromosomes in prometaphase the system exploits the back-to-back geometry of sister kinetochores^{22,23} to create optimal conditions for error correction needed to promote faithful chromosome segregation. The coordinated and decisive switch in k-MT stability that we show at the prometaphase to metaphase transition resembles the decisive switch in k-MT stability described previously during the metaphase to anaphase transition¹⁰ (Fig. 4g). These switches in k-MT attachment stability occur as cyclin proteins drop below threshold levels, with the prometaphase to metaphase transition being regulated by cyclin A and the metaphase to anaphase transition being regulated by cyclin B^{24,25}. Unlike cyclin B, there is no established feedback mechanism to prevent cyclin A destruction in the absence of k-MT attachment¹⁹. This indicates that cyclin A functions as a timer in prometaphase to ensure efficient error correction, consistent with previous data showing a linear relationship between the duration of prometaphase and the level of cyclin A¹². These data define prometaphase and metaphase as biochemically distinct cellular states and show that the prometaphase to metaphase transition is a decisive, unidirectional biochemical event like other phase transitions in the cell cycle^{26–28}.

METHODS SUMMARY

k-MT attachment stability was measured in cultured cells expressing α -tubulin tagged with photoactivatable GFP. DIC microscopy was used to identify mitotic cells and fluorescent images were generated and acquired using Quorum WaveFX-X1 spinning disk confocal system (Quorum Technologies) equipped with Mosaic digital mirror for photoactivation (Andor Technology) and Hamamatsu ImageEM camera. Fluorescence intensities were normalized to the first time point after photoactivation for each cell following background subtraction and correction for photobleaching.

Online Content Any additional Methods, Extended Data display items and Source Data are available in the online version of the paper; references unique to these sections appear only in the online paper.

Received 23 April; accepted 26 July 2013.

Published online 8 September 2013.

- Cimini, D., Moree, B., Canman, J. C. & Salmon, E. D. Merotelic kinetochore orientation occurs frequently during early mitosis in mammalian tissue cells and error correction is achieved by two different mechanisms. *J. Cell Sci.* **116**, 4213–4225 (2003).
- Bakhom, S. F., Thompson, S. L., Manning, A. & Compton, D. A. Genome stability is ensured by temporal control of kinetochore–microtubule dynamics. *Nature Cell Biol.* **11**, 27–35 (2009).
- Lengauer, C., Kinzler, K. W. & Vogelstein, B. Genetic instabilities in human cancers. *Nature* **396**, 643–649 (1998).
- Thompson, S. L. & Compton, D. A. Examining the link between chromosomal instability and aneuploidy in human cells. *J. Cell Biol.* **180**, 665–672 (2008).
- Cimini, D. *et al.* Merotelic kinetochore orientation is a major mechanism of aneuploidy in mitotic mammalian tissue cells. *J. Cell Biol.* **153**, 517–528 (2001).
- Bakhom, S. F., Genovese, G. & Compton, D. A. Deviant kinetochore microtubule dynamics underlie chromosomal instability. *Curr. Biol.* **19**, 1937–1942 (2009).
- Thompson, S. L. & Compton, D. A. Chromosome missegregation in human cells arises through specific types of kinetochore–microtubule attachment errors. *Proc. Natl Acad. Sci. USA* **108**, 17974–17978 (2011).
- Liu, D., Vader, G., Vromas, M. J., Lampson, M. A. & Lens, S. M. Sensing chromosome bi-orientation by spatial separation of aurora B kinase from kinetochore substrates. *Science* **323**, 1350–1353 (2009).
- Nicklas, R. B. & Ward, S. C. Elements of error correction in mitosis: microtubule capture, release, and tension. *J. Cell Biol.* **126**, 1241–1253 (1994).
- Zhai, Y., Kronebusch, P. J. & Borisy, G. G. Kinetochore microtubule dynamics and the metaphase-anaphase transition. *J. Cell Biol.* **131**, 721–734 (1995).
- Pines, J. Mitosis: a matter of getting rid of the right protein at the right time. *Trends Cell Biol.* **16**, 55–63 (2006).
- den Elzen, N. & Pines, J. Cyclin A is destroyed in prometaphase and can delay chromosome alignment and anaphase. *J. Cell Biol.* **153**, 121–136 (2001).
- Skoufias, D. A., Andreassen, P. R., Lacroix, F. B., Wilson, L. & Margolis, R. L. Mammalian mad2 and bub1/bub1 recognize distinct spindle-attachment and kinetochore-tension checkpoints. *Proc. Natl Acad. Sci. USA* **98**, 4492–4497 (2001).
- Manning, A. L. *et al.* CLASP1, astrin and Kif2b form a molecular switch that regulates kinetochore-microtubule dynamics to promote mitotic progression and fidelity. *EMBO J.* **29**, 3531–3543 (2010).
- Kelly, A. E. & Funabiki, H. Correcting aberrant kinetochore microtubule attachments: an Aurora B-centric view. *Curr. Opin. Cell Biol.* **21**, 51–58 (2009).
- DeLuca, K. F., Lens, S. M. & DeLuca, J. G. Temporal changes in Hec1 phosphorylation control kinetochore–microtubule attachment stability during mitosis. *J. Cell Sci.* **124**, 622–634 (2011).
- Gong, D. & Ferrell, J. E. The roles of cyclin A2, B1, and B2 in early and late mitotic events. *Mol. Cell Biol.* **21**, 3149–3161 (2010).
- Mihaylov, I. S. *et al.* Control of DNA replication and chromosome ploidy by Germinin and Cyclin A. *Mol. Cell Biol.* **22**, 1868–1880 (2002).
- Di Fiore, B. & Pines, J. How cyclin A destruction escapes the spindle assembly checkpoint. *J. Cell Biol.* **190**, 501–509 (2010).
- Musacchio, A. & Salmon, E. D. The spindle-assembly checkpoint in space and time. *Nature Rev. Mol. Cell Biol.* **8**, 379–393 (2007).
- Bakhom, S. F. & Compton, D. A. Kinetochore and disease: keeping microtubule dynamics in check! *Curr. Opin. Cell Biol.* **24** (2012).
- Indjeian, V. B. & Murray, A. W. Budding yeast mitotic chromosomes have an intrinsic bias to biorient on the spindle. *Curr. Biol.* **17**, 1837–1846 (2007).
- Loňčáček, J. *et al.* The centromere geometry essential for keeping mitosis error free is controlled by spindle forces. *Nature* **450**, 745–749 (2007).
- Holloway, S. L., Glotzer, M., King, R. W. & Murray, A. W. Anaphase is initiated by proteolysis rather than by the inactivation of maturation-promoting factor. *Cell* **73**, 1393–1402 (1993).
- Surana, U. *et al.* Destruction of the CDC28/CLB mitotic kinase is not required for the metaphase to anaphase transition in budding yeast. *EMBO J.* **12**, 1969–1978 (1993).
- Pagliuca, F. W. *et al.* Quantitative proteomics reveals the basis for biochemical specificity of cell-cycle machinery. *Mol. Cell* **43**, 406–417 (2011).
- Reed, S. I. Ratchets and clocks: the cell cycle, ubiquitylation and protein turnover. *Nature Rev. Mol. Cell Biol.* **4**, 855–864 (2003).
- Trunnell, N. B., Poon, A. C., Kim, S. Y. & Ferrell, J. E. Ultrasensitivity in the regulation of Cdc25 and Cdk1. *Mol. Cell* **41**, 263–274 (2011).

Acknowledgements This work was supported by National Institutes of Health grants GM51542 (D.A.C.) and GM008704 (L.K.) and the John H. Copenhaver Jr and William H. Thomas, MD 1952 Junior Fellowship (L.K.). We thank J. Pines and J. DeLuca for providing reagents.

Author Contributions L.K. and D.A.C. were responsible for experimental design, data interpretation and writing the manuscript. L.K. conducted the experiments.

Author Information Reprints and permissions information is available at www.nature.com/reprints. The authors declare no competing financial interests. Readers are welcome to comment on the online version of the paper. Correspondence and requests for materials should be addressed to D.A.C. (duane.a.compton@dartmouth.edu).

METHODS

Cell culture. RPE-1 (ATCC, CRL-4000), PA (photoactivatable GFP-tubulin-expressing)-RPE-1 (ATCC, CRL-4000), U2OS (ATCC, HTB-96) and PA-U2OS (ATCC, HTB-96) cells, and PA-PtK1 (ATCC, CCL-35) cells were grown in Dulbecco's modified Eagle's medium, (DMEM; Invitrogen) supplemented with 10% FBS (Mediatech), 50 IU ml⁻¹ penicillin and 50 µg ml⁻¹ streptomycin (Mediatech) at 37 °C in a humidified atmosphere with 5% CO₂. All cell lines are validated as mycoplasma free. Media for cells expressing photoactivatable GFP-tubulin was supplemented with G418 (Mediatech). Cells were incubated with 150 µg ml⁻¹ of nocodazole (Millipore) for 12 h and then either released into 5 µM MG132 and analysed through live-cell imaging, or collected through mitotic shake-off and prepared for immunoblots. Cells were incubated with 100 µM monastrol (TOCRIS Bioscience) for 1 h or 6 h and then either analysed through live-cell imaging, prepared for immunofluorescence or released into DMEM for 40 min and prepared for immunofluorescence.

Cell transfection. Plasmid transfections were done with FuGENE 6 (Roche Diagnostics), and cells analysed 12 h later by live-cell imaging, immunofluorescence or preparation for immunoblots. Short interfering RNA transfections were conducted using Oligofectamine (Invitrogen), and cells analysed 48 h later. RNA duplexes for *CCNA2* (5'-CTATGGACATGTCAATTGT-3') and *NUF2* (5'-GCAUGCCGUGAAACGUUA-3') were purchased from Applied Biotechnologies. **Antibodies.** Antibodies used for this study were: ACA (anti-centromere antibody) (CREST; Geisel School of Medicine), actin (Seven Hills Bioreagents, LMAB-C4), astrin¹³, aurora B kinase (Novus Biologicals, NB100-294), BUBR1 (Abcam, ab4637), HEC1 (Novus Biologicals, NB100-338), phospho (p)-HEC1 (provided by Jennifer DeLuca), cyclin A (Santa Cruz Antibodies, sc-751), tubulin (Sigma-Aldrich, T9026), p-H3 (Cell Signaling Technologies, 3377S) and γ -H2AX (Novus Biologicals, NB100-384). Secondary antibodies were conjugated to fluorescein isothiocyanate (FITC) (Jackson ImmunoResearch; anti-mouse, 715-096-151; anti-rabbit, 111-005-003), Texas Red (Jackson ImmunoResearch; anti-mouse, 715-076-020; anti-rabbit, 111-605-045), Cy5 (Invitrogen, anti-human, A-11013) and horseradish peroxidase (Jackson ImmunoResearch; anti-mouse, 715-036-151; anti-rabbit, 211-002-171). Immunoblots were detected using Lumiglow (KPL).

Photoactivation. Images were acquired using Quorum WaveFX-X1 spinning disk confocal system (Quorum Technologies) equipped with Mosaic digital mirror for photoactivation (Andor Technology) and Hamamatsu ImageEM camera. DIC microscopy was used to identify prometaphase and metaphase cells with bipolar spindles. Microtubules were locally activated in one half spindle. Fluorescence images were captured every 15 s for 4 min with a 100 \times oil-immersion 1.4 numerical aperture objective. For measurement of unstable MTs, fluorescence images were captured every 5 s for 1 min. DIC microscopy was then used to verify that a bipolar spindle was maintained throughout image acquisition and that cells had not entered anaphase.

For double photoactivation experiments, prometaphase cells were identified using DIC. Microtubules were locally activated in one half spindle, and DIC was then used to verify that the cell was still in prometaphase. After which, microtubules were again locally activated in either prometaphase or metaphase (identified through DIC). Using DIC, cells were observed continuing through anaphase to ensure cell survival.

To quantify fluorescence dissipation after photoactivation, pixel intensities were measured within a 1-µm rectangular area surrounding the region of highest fluorescence intensity and background subtracted using an equal area from the non-activated half spindle. The values were corrected for photobleaching by treating cells with 10 µM taxol and determining the percentage of fluorescence loss during 4 min of image acquisition after photoactivation. Fluorescence values were

normalized to the first time point after photoactivation for each cell and the average intensity at each time point was fit to a double exponential curve $A1 \times \exp(-k_1 t) + A2 \times \exp(-k_2 t)$ using MatLab (Mathworks), in which t is time, $A1$ represents the less stable non-kinetochore microtubule population and $A2$ the more stable kinetochore microtubule population with decay rates of k_1 and k_2 , respectively. The turnover half-life for each process was calculated as $\ln 2/k$ for each population of microtubules.

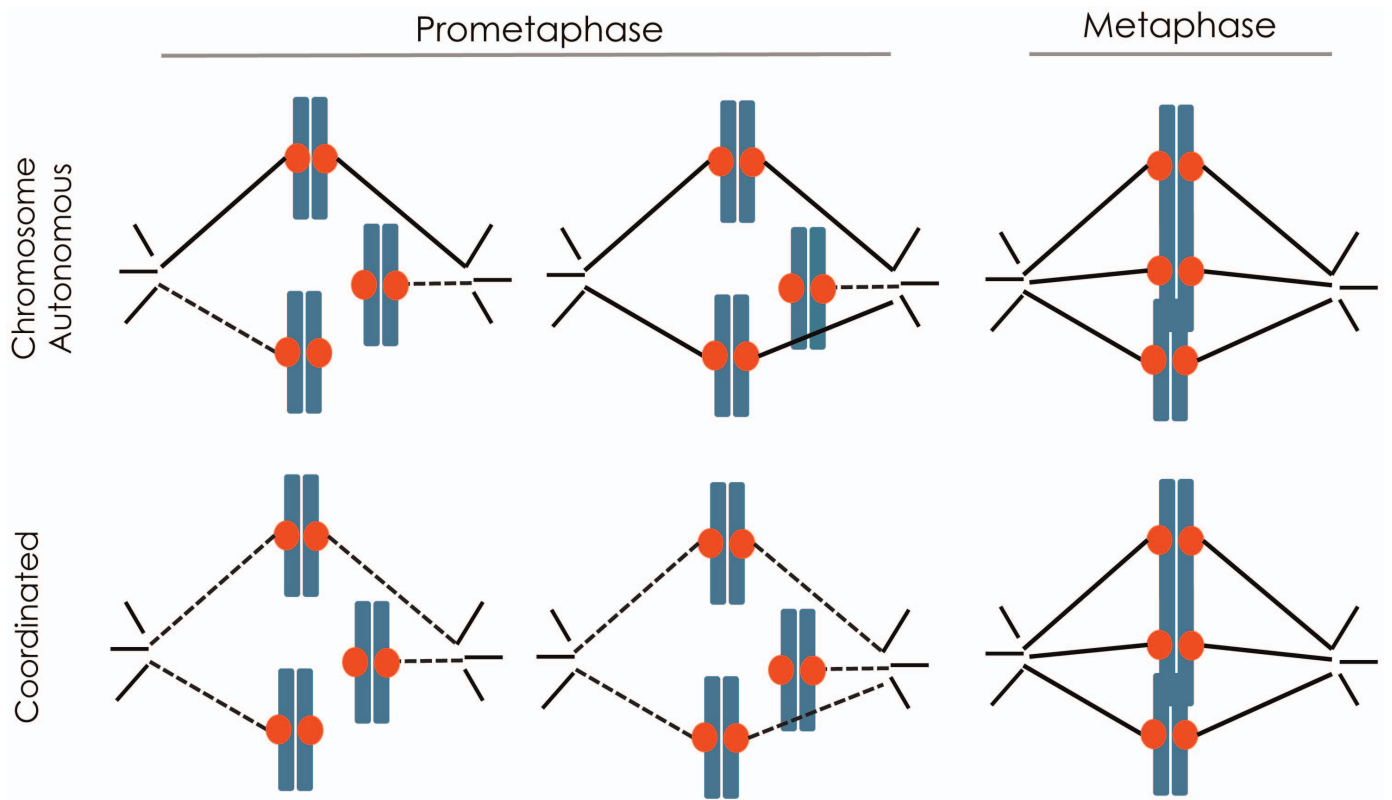
Immunofluorescence microscopy. Cells were fixed with 3.5% paraformaldehyde for 15 min, washed with Tris-buffered saline with 5% bovine serum albumin (TBS-BSA) and 0.5% Triton X-100 for 5 min and TBS-BSA for 5 min. Antibodies were diluted in TBS-BSA plus 0.1% Triton X-100 and coverslips incubated for 12 h at 4 °C. After which, cells were washed with TBS-BSA for 5 min with shaking. Secondary antibodies were diluted in TBS-BSA plus 0.1% Triton X-100 and coverslips incubated for 1 h at room temperature (20–25 °C). For p-HEC1, all wash buffers were supplemented with 80 nM okadaic acid and 40 nM microcystin. Images were acquired with Orca-ER Hamamatsu cooled charge-coupled device camera mounted on an Eclipse TE 2000-E Nikon microscope. 0.2 µm optical sections in the z -axis were collected with a plan Apo 60 \times 1.4 numerical aperture oil immersion objective at room temperature. Iterative restoration was performed using Phylum Live software (Improvision). Anaphase chromatids were counted as lagging if they contained centromere staining (using CREST antibody) in the spindle midzone separated from centromeres at the poles. The scoring of lagging chromosomes in anaphase was performed blinded. The investigator was not aware of which sample they were counting until all samples were completed and subsequently unblinded.

For quantitative assessments, cells were fixed and stained for aurora B/p-HEC1, CREST and DNA. Pixel intensities for CREST and aurora B/p-HEC1 staining were measured in approximately 15 regions over the entire cell. Background fluorescence was subtracted and the ratio of intensities were calculated and averaged over multiple kinetochores from multiple mitotic cells ($n \geq 10$ cells). To quantify DNA condensation, DAPI fluorescence was measured in approximately five regions over the entire cell. Background fluorescence was subtracted, and the ratio was averaged over multiple cells ($n \geq 10$ cells per condition).

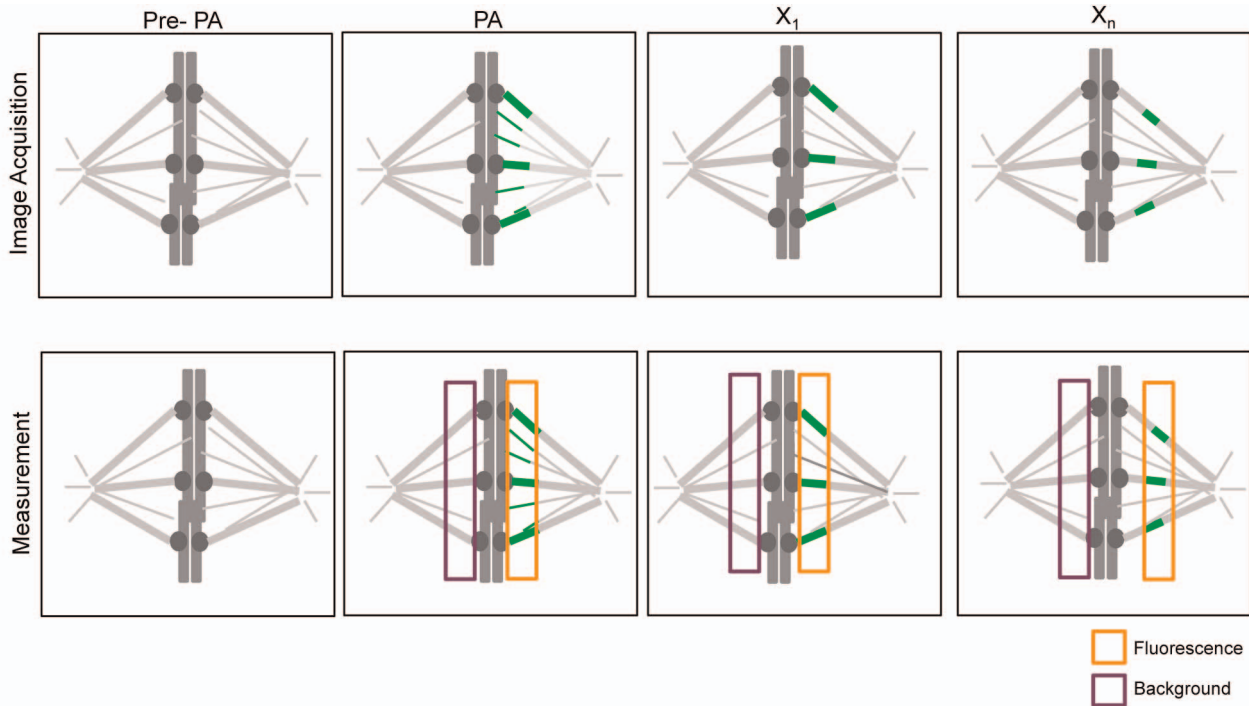
Measurements of intercentromere distances were made with Huygens Essential software. All measurements were performed for three independent experiments. Error bars represent standard errors (s.e.m.). The Student's t -test was used to calculate the significance of differences between samples.

For endogenous cyclin A staining and quantification, Cells were fixed with PBS with 3.5% paraformaldehyde and 2% sucrose for 10 min. After which, cells were permeabilized with ice-cold methanol for 5 min and subsequently washed with 500 mM ammonium chloride in PBS for 20 min twice. Cells were then incubated with PBS with 2% donkey serum for 1 h. After which, cells were incubated with primary and secondary antibodies. Quantification of cyclin A levels were done using ImageJ (National Institutes of Health). The cytoplasm of a G1 cell (identified by the lack of cyclin A in the nucleus) was used to measure fluorescence intensity and was then used for background subtraction.

Statistical analysis. For photoactivation, no fewer than ten cells were used for each condition, which is sufficient to detect significant differences when the effect size is twofold or more. For scoring lagging chromosomes and measuring differences in fluorescence intensity, no fewer than 20 cells per condition, which is sufficient to detect significant differences between samples, were used. Data analysis was performed blind. The investigator was unaware of which sample they were counting until all samples were completed and subsequently unblinded. All data had a normal distribution, with similar variance between all conditions tested. Two-tailed t -tests were conducted where indicated in the figure legends.



Extended Data Figure 1 | Models of k-MT attachment stability. Unstable (dotted lines) and stable (solid lines) k-MT depict the differences in the chromosome-autonomous and -coordinated models of regulating k-MT attachment stability.

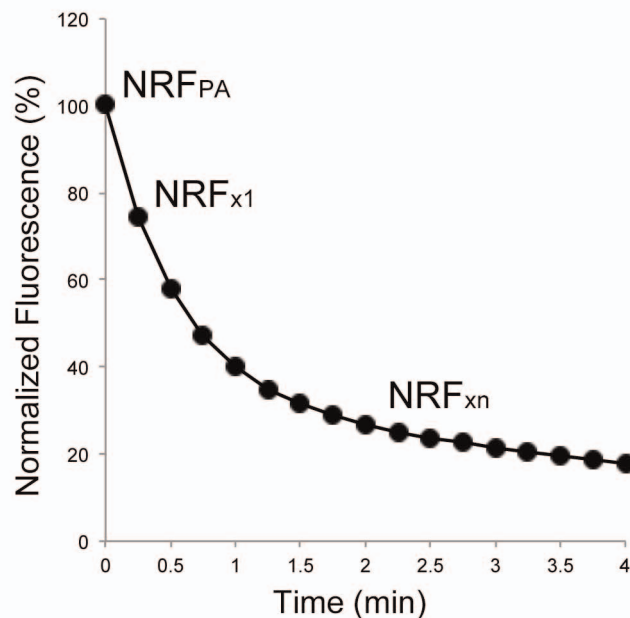


Relative Fluorescence (RF) = Fluorescence - Background

Normalized Relative Fluorescence $PA = (RF_{PA} \times \text{Bleaching Coefficient})/RF_{PA}$

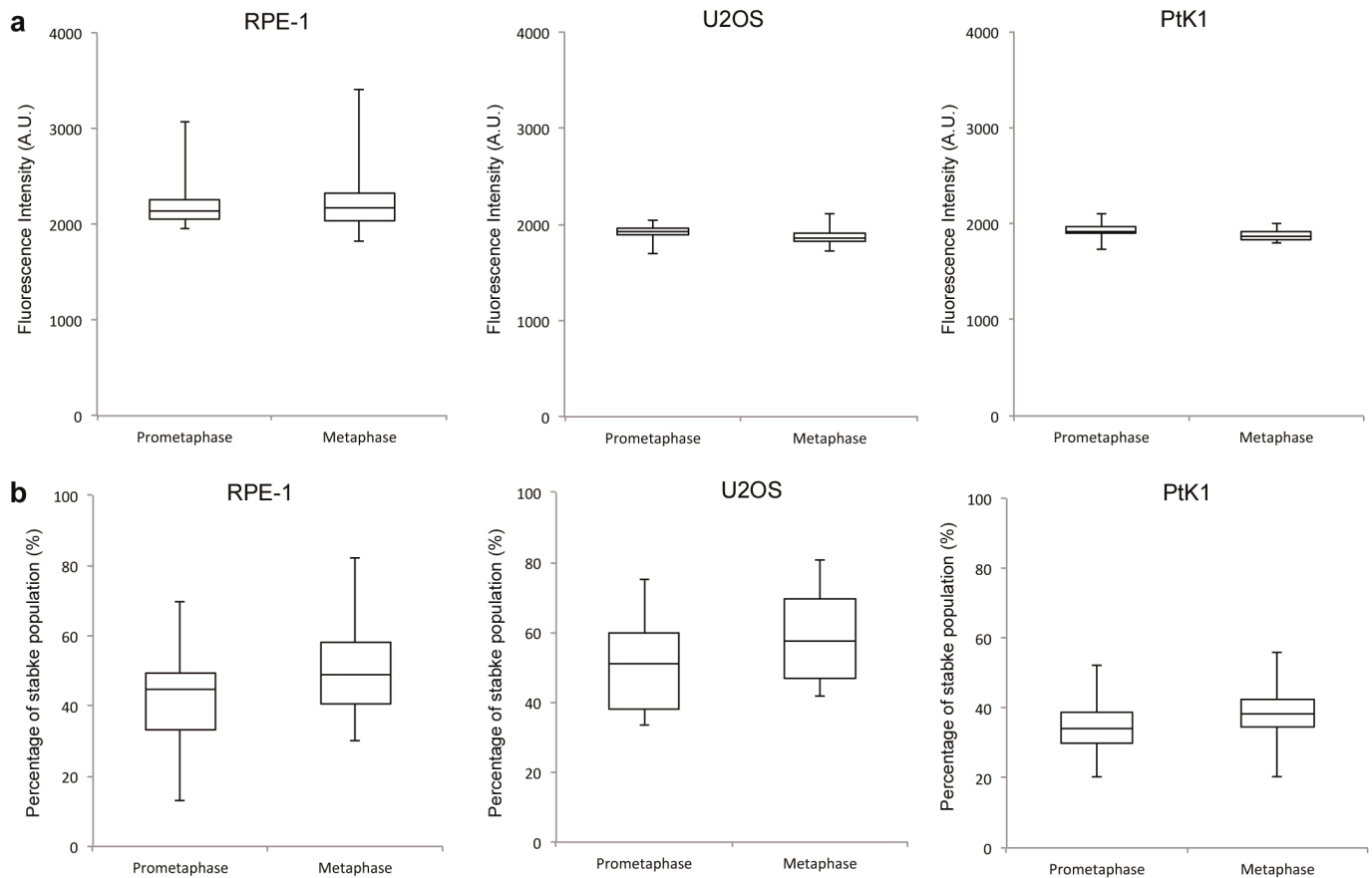
Normalized Relative Fluorescence $x_1 = (RF_{x_1} \times \text{Bleaching Coefficient})/RF_{PA}$

Normalized Relative Fluorescence $x_n = (RF_{x_n} \times \text{Bleaching Coefficient})/RF_{PA}$



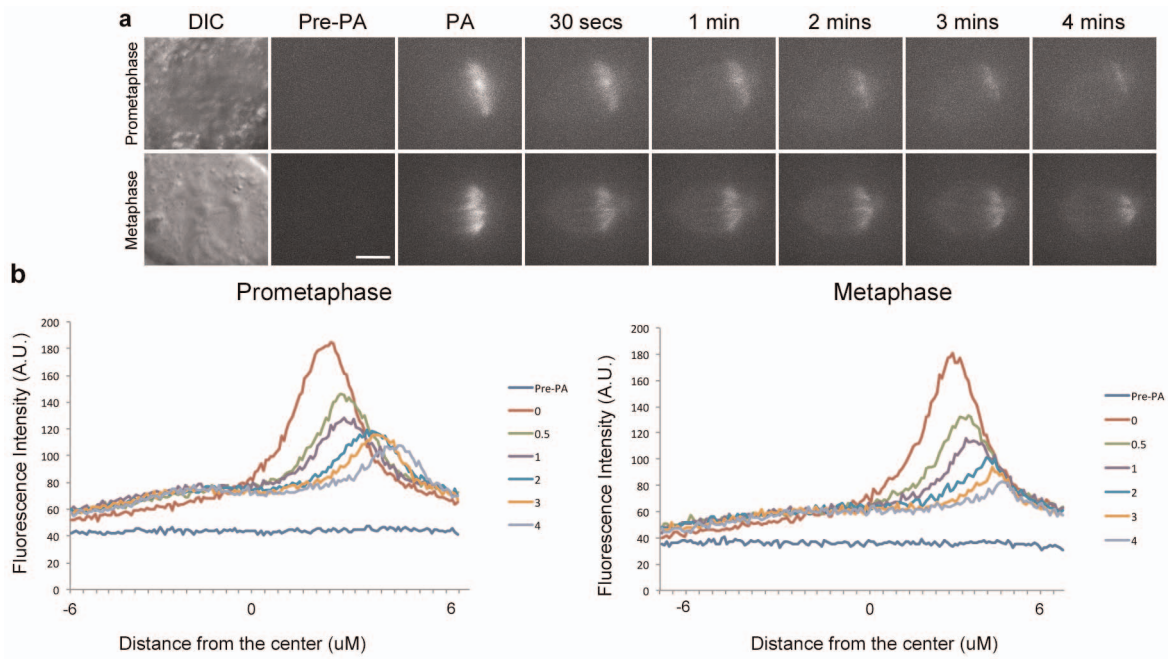
Extended Data Figure 2 | Schematic of methods for quantification of photoactivation. Relative fluorescence (RF) is calculated by subtracting fluorescence of an equal size region on the non-photoactivated half-spindle (background) from the fluorescence intensity of the photoactivated half-spindle (fluorescence). Bleaching coefficient is determined for each time point

using taxol-treated cells. Normalized relative fluorescence is then calculated by multiplying the relative fluorescence of individual time points by the bleaching coefficient, divided by the relative fluorescence of the first photoactivated time point (RF_{PA}). The data fits into a double exponential curve.



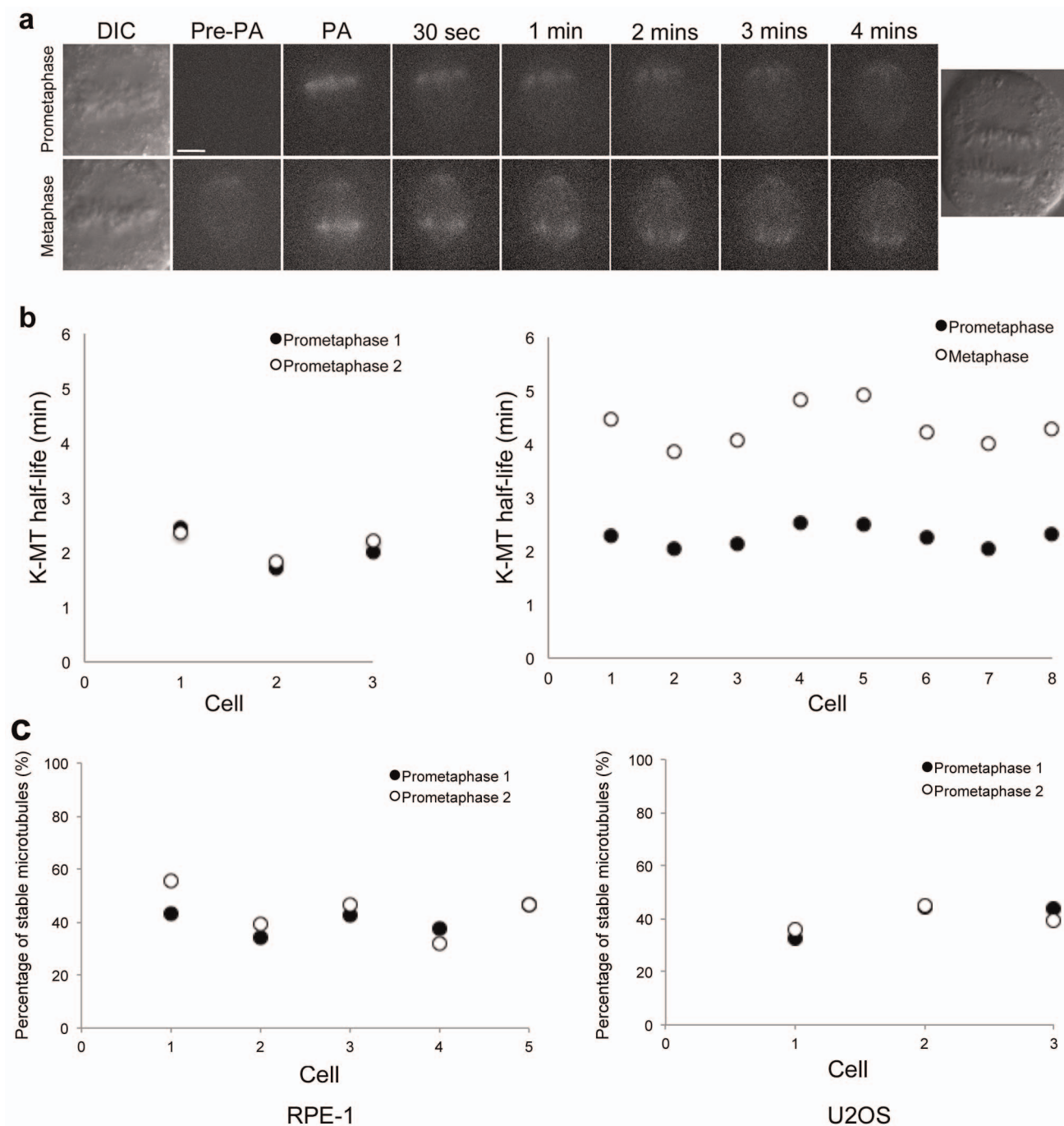
Extended Data Figure 3 | Fluorescence intensity and percentage of MTs in the stable population. **a**, Box and whisker plots of fluorescence intensity of photoactivatable GFP-tubulin after photoactivation. **b**, Percentage of MTs in

the stable population (for example, k-MTs) calculated from the exponential decay curve of photoactivated fluorescence ($R^2 > 0.99$); $n = 40$ cells for RPE-1 and U2OS, and 20 cells for PtK1 per condition.



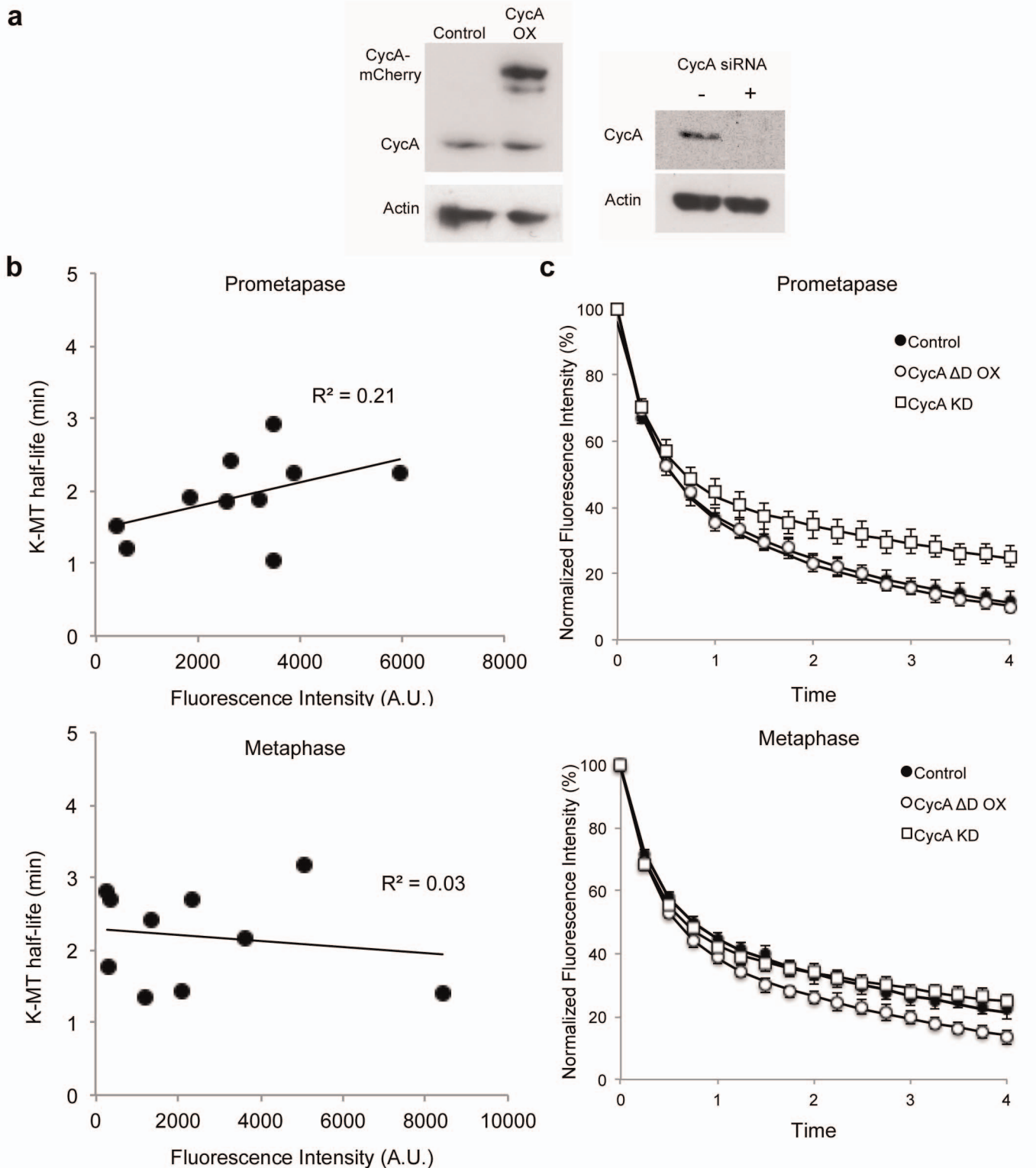
Extended Data Figure 4 | Poleward microtubule flux. **a**, DIC and time-lapse fluorescence images of an individual U2OS cell in prometaphase (top) and

metaphase (bottom). Scale bar, 5 μm . **b**, fluorescence intensity linescan of spindles shown in **a**.



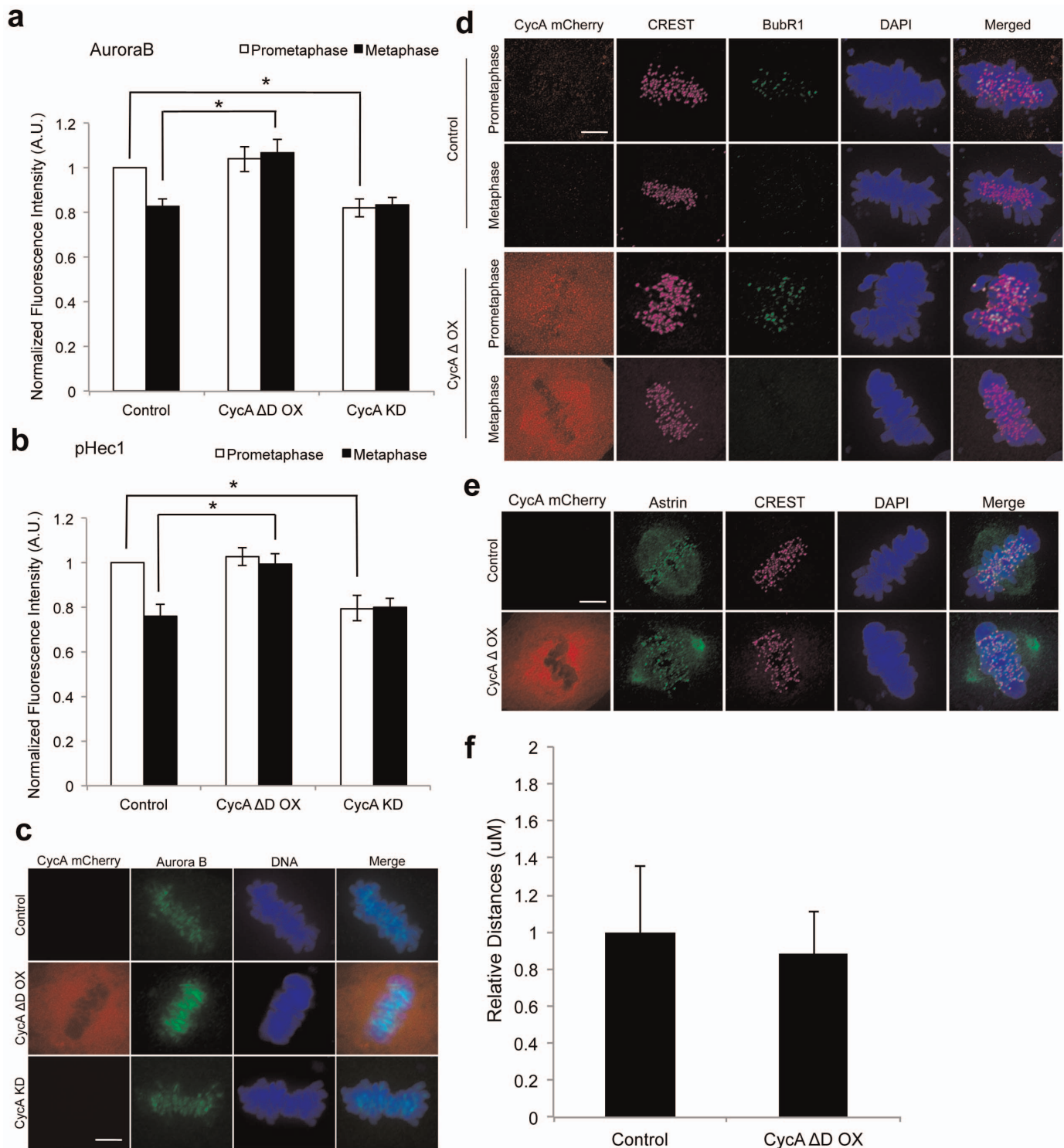
Extended Data Figure 5 | Single-cell measurements in U2OS cells. **a**, DIC and time-lapse fluorescence images of an individual U2OS cell in prometaphase and then in metaphase. Scale bar, 5 μ m. **b**, k-MT half-life of individual U2OS cells photoactivated serially in prometaphase (left) or in prometaphase and

then again in metaphase (right). **c**, Percentage of MTs in the stable population (for example, k-MTs) calculated from the exponential decay curve of serially photoactivated prometaphase fluorescence ($R^2 > 0.99$).



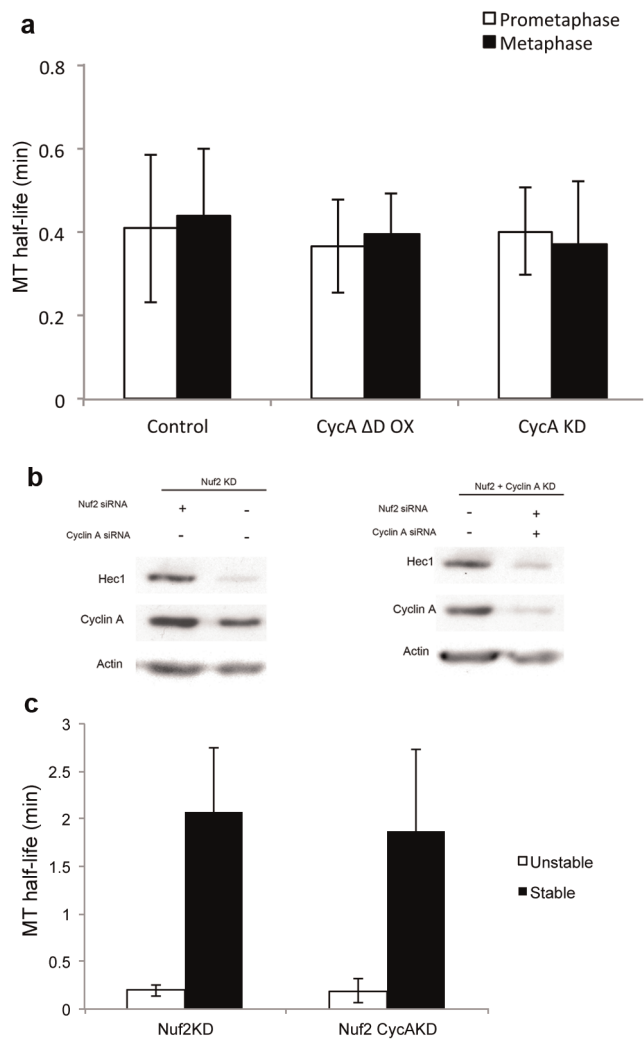
Extended Data Figure 6 | Manipulation of cyclin A levels. **a**, Western blots of cyclin-A-overexpressing (left) and cyclin-A-depleted (right) U2OS cells compared to control. siRNA, short interference RNA. **b**, Cyclin A(Δ D)-mCherry fluorescence intensity and respective k-MT half-life of U2OS cells photoactivated in prometaphase (top) and metaphase (bottom). Linear fit with

R^2 value. **c**, Normalized fluorescence over time after photoactivation of untreated U2OS (control), U2OS cells overexpressing cyclin A(Δ D)-mCherry (CycA(Δ D)OX) and depleted of cyclin A (CycA KD); $n = 13$ cells for control and 10 cells for CycA(Δ D)OX and CycA KD per condition.

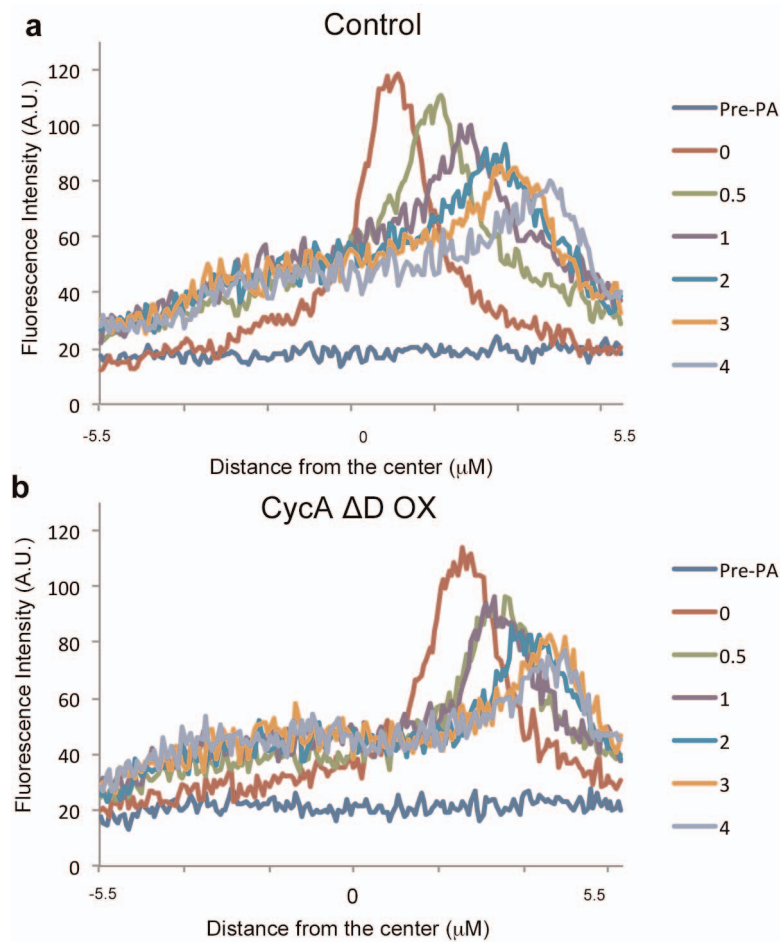


Extended Data Figure 7 | Mitotic properties of cells with altered levels of cyclin A. Immunofluorescence of prometaphase and metaphase untreated U2OS (control) and cyclin A($\Delta\Delta$)-overexpressing U2OS cells. **a**, Fluorescence intensities of centromeres stained for aurora B kinase in U2OS cells normalized using CREST in both prometaphase and metaphase. **b**, Fluorescence intensities of centromeres stained for phosphor (p)-HEC1 in U2OS cells normalized using CREST in both prometaphase and metaphase. **c**, Immunofluorescence of untreated metaphase U2OS (control), U2OS cells overexpressing cyclin A($\Delta\Delta$)-mCherry and depleted of cyclin A. Scale bar, 5 μm . Graphs show

mean \pm s.e.m. from 20 cells per condition from three independent experiments. $*P \leq 0.01$, two-tailed *t*-test. **d**, Localization of BUB1B in prometaphase and metaphase cells with and without (control) expression of cyclin A($\Delta\Delta$). **e**, Localization of astrin in metaphase cells with and without (control) expression of cyclin A($\Delta\Delta$); $n = 30$ cells per condition from three independent experiments. Scale bar, 5 μm . **f**, Intercentromere distances of untreated and cyclin A($\Delta\Delta$)-overexpressing U2OS cells; $n = 30$ cells per condition from three independent experiments. Graphs show mean \pm s.e.m. $*P \leq 0.01$, two-tailed *t*-test.

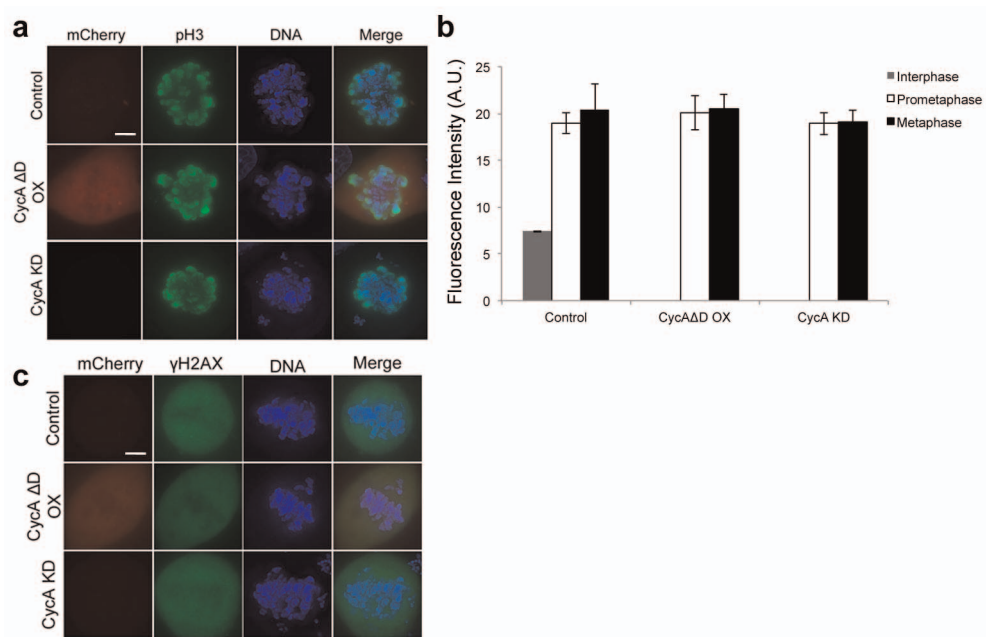


Extended Data Figure 8 | k-MT are selectively influenced by cyclin A. **a**, MT half-life of untreated (control), cyclin-A-overexpressing and cyclin-A-depleted prometaphase and metaphase U2OS cells measured at 5-s intervals for 1 min; $n = 10$ cells per condition. **b**, western blots of NUF2-depleted (left) and NUF2- and cyclin-A-depleted (right) U2OS cells compared to control U2OS cells. **c**, MT half-life of NUF2-depleted and NUF2- and cyclin-A-depleted U2OS cells; $n = 10$ cells per condition. Graphs show mean \pm s.e.m.



Extended Data Figure 9 | Poleward flux in cells expressing mutant cyclin A. Linescan analysis measuring fluorescence intensity of metaphase spindles in

untreated (control) and cyclin A overexpression in photoactivatable GFP-tubulin-expressing U2OS cells.



Extended Data Figure 10 | Properties of mitotic cells expressing mutant cyclin A. Immunofluorescence of untreated metaphase U2OS cells (control), U2OS cells overexpressing cyclin A(ΔD)–mCherry and U2OS cells depleted of cyclin A (CycA KD). Scale bar, 5 μm . **b**, Fluorescence intensities of DNA

stained with DAPI in U2OS cells in both prometaphase and metaphase. Scale bar, 5 μm ; $n = 60$ cells per condition from three independent experiments. Graphs show mean \pm s.e.m.